Available online at www.sciencedirect.com
ScienceDirect
Energy Reports 7 (2021) 1504–1512
www.elsevier.com/locate/egyr

2021 International Conference on Energy Engineering and Power Systems (EEPS2021), August 20–22, 2021, Hangzhou, China

Study on enhanced heat transfer characteristics of metal foam solar receiver in Solar Power Tower plants

Chen Kang[a,b,*], Wang Xiao[a], Chen Pengfei[a], Wen Long[a]

[a] *Institute of solar engineering technology, Northwest Engineering Corporation Limited, PowerChina, Xi'an 710065, China*
[b] *State Key Laboratory of Multiphase Flow in Power Engineering, Xi'an Jiaotong University, Xi'an 710049, China*

Received 18 September 2021; accepted 20 September 2021

Abstract

In order to explore the mechanism of heat and mass transfer of metal foam absorber based on electrodeposition, the numerical simulation study of metal foam absorbers with different structures was carried out, and the heat transfer model of the coated metal foam tube bundle with a tube spacing of 3D × 1.5D was analyzed and established. Compared with the smooth tube bundle, with the *Re* number varying from 100 to 1500, the R_{ext} of the tube bundle coated with stainless steel foam decreased from 0.061 K/W to 0.009 K/W, and the thermal resistance ratio outside the tube increased from 2.75 to 4.76. The pressure loss of the tube rose from 1.89 Pa to 80.10 Pa, and the pressure loss outside the tube dropped from 5.15 to 3.12. The overall performance index PEC of the tube increased from 1.59 to 3.26. Compared with rows of staggered tube bundles from 2.5D to 2.2D, the heat transfer coefficient can reach 4621 W/m^2/K and the pressure loss is 1.67%.

Peer-review under responsibility of the scientific committee of the International Conference on Energy Engineering and Power Systems, EEPS, 2021.

Keywords: Metal foam; Heat transfer enhancement; Solar receiver

1. Introduction

In the light concentrating and heat collecting system of Solar Power Tower Station, the heat absorber is responsible for converting solar energy into heat energy. However, due to the uneven solar radiation, the efficiency of light-to-heat conversion is greatly restricted by system safety, so the need of improving quality and efficiency is urgent. Metal foam has the advantages of low density (2% to 10% of the same material), high rigidity and large specific surface area (up to 2000–10 000 m^2/m^3). The solid skeleton in metal foam enlarges its contact area with the fluid surface, increases the disturbance of the fluid, so as to improve the heat transfer effectively. Metal foam has widespread applications on the industrial fields such as pipe heating of metal components, fuel cell and

* Corresponding author at: Institute of solar engineering technology, Northwest Engineering Corporation Limited, PowerChina, Xi'an 710065, China.
E-mail address: chen_kang@xjtu.edu.cn (K. Chen).

https://doi.org/10.1016/j.egyr.2021.09.092

Peer-review under responsibility of the scientific committee of the International Conference on Energy Engineering and Power Systems, EEPS, 2021.

hydrogen storage materials [1–4]. Therefore, the applications of metal foam to raise the heat transfer capability of heat absorber and reduce operational risk of heat receiver has become a new trend of solar thermal utilization technology in recent years.

Calmidi and Mahajan [5,6] studied the process of forced convection heat transfer of aluminum foam filled flat channel, which has a porosity of 0.89–0.97, through experiments and numerical simulations. The empirical formula of effective thermal conductivity of metal foam was obtained through experiments, and the performance of heat exchanger which used metal foam as fins was predicted. Numerical simulation research used a non-thermal equilibrium model, and it was found that the influence of thermal dispersion effect could be ignored when air was used as the working fluid. Based on the research of Calmidi and Mahajan [5,6], Tamayol [7] and Hooman [8] have established the thermal resistance mesh model, simulating the forced convection heat transfer of metal foam, and they have defined the effective heat transfer coefficient which only depends on the material property parameters and the thermal conductivity of the fluid. Kim [9,10] et al. conducted an experimental study on the forced convection heat transfer of a rectangular metal foam channel with water as the cooling medium and concluded the empirical correlation between the resistance coefficient and the heat transfer coefficient of the rectangular channel heat exchanger. Zhao and Kim et al. [11,12] studied the convection heat transfer of metal foams in 12 flat channels with different structural parameters by experiments and numerical simulations. It was found that the pore density had a greater influence on the heat transfer performance of ferroalloy foam, while the heat transfer performance of copper foam was more easily affected by porosity.

However, with the rapid change of the preparation process of metal foam, new characteristics will appear. Mancin et al. [13–16] have carried out a series of experimental studies on copper foam filled and aluminum foam filled flat plates, and different flow and heat transfer characteristics were obtained. For example, the pressure loss increases with the increase of porosity; the pore density has little effect on the performance of the heat exchanger, etc. Due to the complex structure of metal foam coated tubes, analytical solutions cannot be obtained. Besides, numerical simulation involves porous-solid coupling and porous-fluid coupling. So far, most of the researches have been focused on flat plate foam and filling foams in circular tubes. Only a few researchers have conducted preliminary studies on the metal foam coated tubes.

Odabaee [17] used 5 groups of aluminum alloy foam materials with different porosities and pore densities to numerically simulate the flow and heat transfer of a single circular tube coated with metal foam. The *j/f* factors of different foam layer thicknesses were obtained when the fluid velocities were 2.8 m/s and 5.6 m/s, which provided a basis for the design of heat transfer of single tube. Odabaee [18] also conducted a numerical simulation study on the forced convection heat transfer of the 4-row staggered aluminum alloy foam coated circular tube. The influence law of Re number, foam layer thickness and tube bundle transverse pitch X_T on heat transfer factor j and resistance coefficient f was obtained. However, the local heat equilibrium model to simulate the convective heat transfer process between the metal framework and the fluid in the coupling phenomenon of the porous medium and the pure fluid region, which would cause a certain error from the actual result. C. T'Joen [19] explored the heat transfer performance of the single-row tube bundle coated with metal foam layers. It was found that with the increase of the thickness of the metal foam layer and the decrease of the tube spacing, the thermal resistance of the tube decreased correspondingly, and the flow resistance outside the tube increased. However, the heat transfer coefficient and resistance characteristics outside the tube also showed results that were completely opposite to the theoretical analysis.

In order to explore the heat and mass transfer mechanism of the solar receiver with a metal foam layer coated circular tube bundle as a heat exchanger, a numerical simulation study of solar receiver under different structures and conditions is conducted in this paper.

2. Tube bundle model and numerical method

2.1. Tube bundle model

In this paper, we select the circular tube with the diameter of 0.95 mm (d_o), the length of 40 mm (L), and are staggered in equilateral triangles. The nitrogen outside the tube traverses the tube bundle from top to bottom, while the nitrogen inside the tube flows from the inside to the outside, and the gas inside and outside the tube forms a cross flow for forced convection heat transfer.

Under the same heat exchange space and working conditions, numerical simulations are carried out on the smooth tube bundle and the new type heat exchange tube bundle. As shown in Fig. 1, the physical model of the new type tube bundles is illustrated.

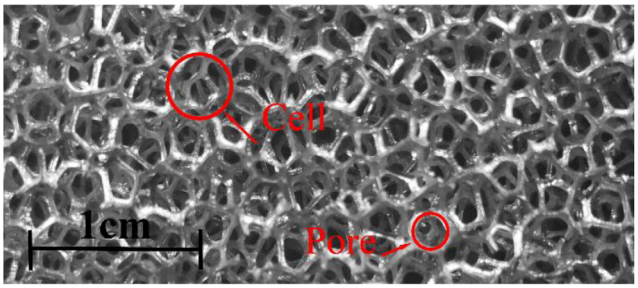

Fig. 1. Structural diagram of metal foam.

2.2. Mathematical model

The physical models of metal foam coated circular tubes and tube bundles include two areas, pure fluid and porous medium. In this paper, the corresponding governing equations are given for two different regions.

Continuity Equation

$$\nabla(\rho\vec{U}) = 0 \tag{1}$$

Momentum Equation

$$\frac{1}{\varepsilon}\left\langle(\vec{U}\cdot\nabla)\rho_f\vec{U}\right\rangle = -\nabla\langle p\rangle_f + \frac{\mu_f}{\varepsilon}\nabla^2\left\langle\vec{U}\right\rangle - \xi\left(\frac{\mu_f}{K} + \frac{\varepsilon F}{\sqrt{K}}\rho_f\left|\left\langle\vec{U}\right\rangle\right|\right)\left\langle\vec{U}\right\rangle \tag{2}$$

Among them, $\langle\ \rangle$ is average volume; ε is porosity; P is pressure; F inertial factor; K is permeability of the metal foam; V is velocity; ρ is density; f is fluid; μ is dynamic viscosity; when $\zeta = 1$, it is the momentum equation of the metal foam region; when $\zeta = 0$, it is the momentum equation of the pure fluid region. The last two terms on the right side of the momentum equation are Darcy's first order term and Forchheimer's second order term.

For the energy description of the heat transfer process in metal foams, two models are generally recognized, the local equilibrium model (LTE) and the local non-equilibrium model (LTNE). In the equilibrium model, the local temperature between the metal skeleton and the fluid is regarded as equal, and an equation is used to describe the energy change between the fluid and the solid. The non-equilibrium model distinguishes the fluid phase from the solid phase, and uses different equations to describe the temperature changes of the fluid and the solid respectively. In this paper, the local non-equilibrium model (LTNE) is adopted to simulate.

Energy Equation of Equilibrium Model:

$$\frac{\partial}{\partial t}(\varepsilon\rho_f E_f + (1-\varepsilon)\rho_s E_s) + \nabla\cdot(\vec{u}(\rho_f E_f + p)) = \nabla\cdot\left[k_{eff}\nabla T - \left(\sum_i h_i J_i\right) + (\tau\cdot\vec{u})\right] \tag{3}$$

The energy equation of non-equilibrium model is divided into fluid phase and solid phase, where the fluid phase energy equation is as follows:

$$\frac{\partial}{\partial t}(\varepsilon\rho_f E_f) + \nabla\cdot(\vec{u}(\rho_f E_f + p)) = \nabla\cdot\left[\varepsilon k_f\nabla T_f - \left(\sum_i h_i J_i\right) + (\tau\cdot\vec{u})\right] + h_{sf}a_{sf}(T_s - T_f) \tag{4}$$

The energy equation of solid phase is as follows:

$$\frac{\partial}{\partial t}((1-\varepsilon)\rho_f E_f) = \nabla\cdot[(1-\varepsilon)\,k_s\nabla T_s] + h_{sf}a_{sf}(T_f - T_s) \tag{5}$$

where k_{eff} is the effective thermal conductivity, which is defined as:

$$k_{eff} = k_{fe} + k_{se} = \varepsilon k_f + (1-\varepsilon)\,k_s \tag{6}$$

Among them, *fe* is effective value for the fluid; *se* is effective value for the solid; T_f is the temperature of fluid phase and T_s is the temperature of solid phase. h_{sf} is the convective heat transfer coefficient of the fluid–solid interface in the metal foam, and the heat transfer between the inner microstructure of the metal foam can be simplified as the forced convection heat transfer of the fluid across the staggered tube bundles. According to the empirical formula of Zukauskas' cross-swept staggered tube bundle, the h_{sf} with the skeleton diameter d_f as the characteristic length can be obtained:

$$h_{sf} = \begin{Bmatrix} 0.76\dfrac{k_f}{d_s} Re_f^{0.4} Pr_f^{0.37} (1 \le Re_f \le 40) \\ 0.52\dfrac{k_f}{d_s} Re_f^{0.5} Pr_f^{0.37} (40 \le Re_f \le 1000) \\ 0.26\dfrac{k_f}{d_s} Re_f^{0.6} Pr_f^{0.37} (1000 \le Re_f \le 2 \times 10^5) \end{Bmatrix} \tag{7}$$

where $Re_f = \rho u d_f / \mu$.

In this paper, ANSYS FLUENT 14.5 numerical calculation software is used, the control equation is discretized by finite volume method, the Standard format is selected for the pressure interpolation format, the SIMPLE algorithm is used for the pressure–velocity coupling, and the other items are discretized by the second-order upwind style. The iteration error is less than 1.0×10^{-6} as the convergence condition, and the influence of radiation heat transfer is ignored.

2.3. Boundary conditions

The boundary conditions of bundle side: assume that the inlet velocity is uniform and the nitrogen enters the inlet section perpendicularly; the inlet temperature is uniform, and $T_{in\text{-}out}$ is 793 K. The pressure inlet and outlet is used as the boundary condition for the inlet and outlet of nitrogen. The outlet pressure outside the tube is 1 atm, and the mass flow $m_{in\text{-}out}$ of the inlet nitrogen outside the tube is 0.0225 kg/s.

The boundary conditions of tube side: assume that the inlet velocity is uniform and the nitrogen enters the inlet section perpendicularly; the inlet temperature is uniform, and $T_{in\text{-}in}$ is 188 K. The pressure inlet and outlet is used as the boundary condition for the inlet and outlet of nitrogen. The outlet pressure in the tube is 10 MPa, and the mass flow $m_{in\text{-}in}$ of the inlet nitrogen inside the tube is 0.0252 kg/s.

The left and right walls of the outer region are symmetrical boundaries. The inner and outer walls of the circular tube and the front and back of the outer section are treated as solid walls, and non-slip adiabatic boundary conditions are adopted. Porous medium is set in the porous medium area.

3. Experimental results and discussion

3.1. Tube spacing

In this paper, numerical simulations are carried out on the flow field and temperature field of the smooth tube bundle and the new heat transfer tube bundle under different Reynolds numbers. Here, taking $Re = 153$ as an example, the heat transfers and flow conditions in these two tube bundle structures are compared and analyzed.

A section perpendicular to the Z axis at $z = 20$ mm, which is 1/2 of the tube length is made, and the temperature distribution cloud diagrams of the two heat transfer models on this section are generated. As shown in Fig. 3. The temperature of the thermal fluid gradually decreases from top to bottom. Comparing Fig. 3(a) and (b), it can be seen that in the smooth tube bundle model, the temperature of the hot fluid after flowing through 8 rows of heat transfer tubes is similar to the temperature of that flowing through 5 rows in the new heat transfer tube bundle model. It shows that the heat transfer capacity of the latter is stronger than that of the former. The reduction in the number of heat transfer tubes not only reduces the area of the heat transfer, but also greatly lowers the difficulty of welding.

When $Re = 153$, the performance parameters of the two tube bundle structures are compared, as shown in Table 1. It can be seen from the table that the thermal fluids under the two models have the same inlet temperature of 793 K. The tube bundle of the new type heat transfer tube can make the temperature of hot fluid drop to 452 K with a temperature difference of 341 K. While the smooth tube bundle can only make the temperature drop to 487 K, and the temperature difference is 306 K. It shows that the heat transfer ability of the new type heat transfer

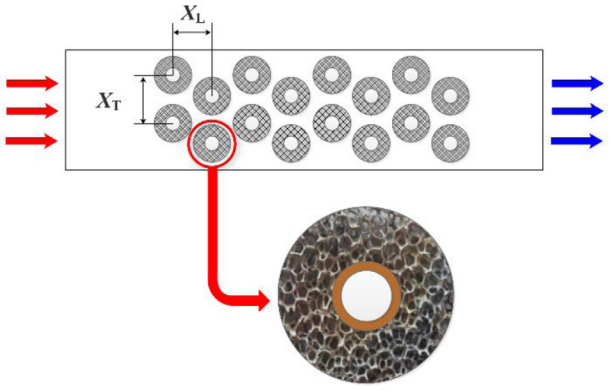

Fig. 2. Physical model of staggered tube bundle.

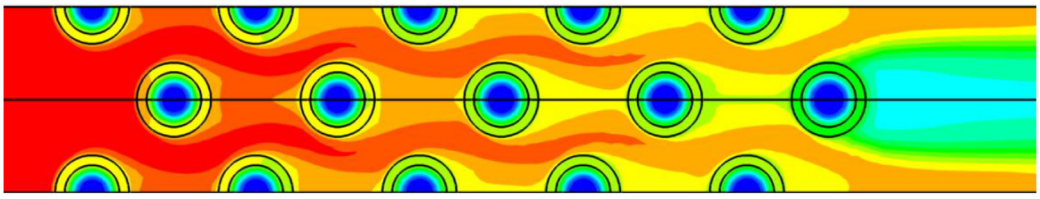

(a) Smooth Tube Bundle

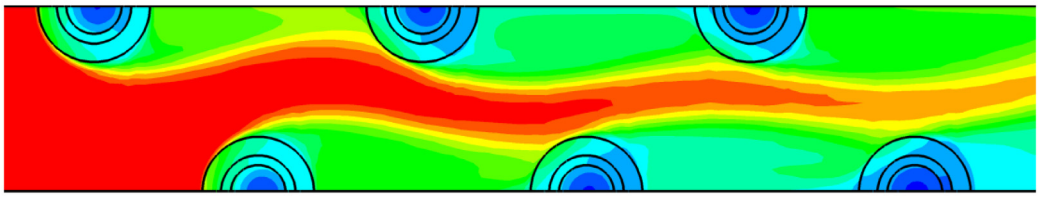

(b) New Type Heat Transfer Tube Bundle

Fig. 3. Temperature field distribution.

Table 1. Comparison of heat transfer performance of the two kinds of tube bundles.

Parameter	Smooth tube bundle	Metal foam tube bundle
Inlet temperature (K)	793	793
Outlet temperature (K)	487	452
Heat transfer rate Q(W)	79.18	111.57
Average heat transfer coefficient (W/(m^2 K))	842	1631
Pressure drop on shell-side (Pa)	5315	1693
Pressure loss (%)	5.25	1.67
Heat transfer weight ratio (MW/kg)	1.23	1.59

tube bundle is better than that of the smooth tube bundle, which can also be directly obtained from the comparison of heat transfer Rates and coefficients.

Since the distance between the new type heat transfer tubes is twice that of the smooth tube bundle, so under the premise of same inlet flow, the pressure drop of the new type heat transfer tube bundle is 1693 Pa, while that of the smooth tube bundle is 5315 Pa, which is far greater than the former. The corresponding pressure loss reduces from 5.25% of the smooth tube bundle to 1.67%.

Although the new type heat transfer tube is made of smooth tube coated with metal foam inside and outside the tube, the weight of the new type heat transfer tube has not increased a lot due to the porosity of the coating metal

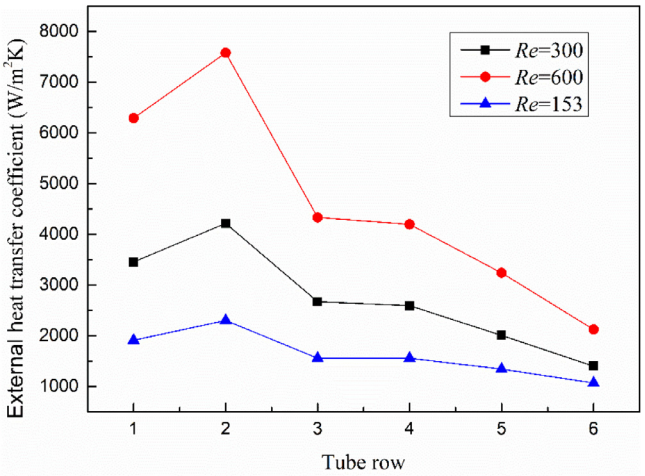

Fig. 4. Variation of heat transfer coefficient with tube row.

foam is as high as 95%. On the contrary, because of the existence of metal foam, the turbulence level of the fluid is greatly increased, and the thermal conductivity of the solid skeleton is very high, the heat transfer Rate of the new type heat transfer tube coated with metal foam is obviously greater than that of the smooth tube. The final calculation shows that the heat transfer Rate to weight ratio of the new type heat transfer tube bundle is 1.59, which is greater than 1.23 of the smooth tube bundle.

It can be seen from Fig. 4 that the variation of heat transfer coefficient with tube row is basically the same at different Reynolds numbers. The heat transfer coefficient of the second row of the tubes is the highest, and the coefficient of other tubes decreases with the deepening of the tube row. The reason is that the second row of tubes is impacted by the fluid most. The flow velocity outside the tube is the highest, and the heat transfer effect is the strongest. With the increase of the depth of the tube row, the temperature of the hot fluid becomes lower and lower, so is the temperature difference between the hot fluid and the cold fluid in the tube, and the driving force of the heat transfer also weakens gradually. Therefore, the deeper the tube row, the lower the heat transfer coefficient.

In addition, with the Reynolds number growth, the heat transfer coefficient of each tube row increases obviously. When the Reynolds number is 600, the average coefficient reaches 4621 W/m^2/K.

3.2. Microstructure characteristics of metal foam

The structure and performance parameters of metal foam materials include porosity, pore diameter d_p, fiber diameter d_f, pore density PPI, specific surface area a_{sf} and permeability K. The specific surface area determines the heat transfer performance. The larger the specific surface area, the better the heat transfer performance. The permeability determines the flow resistance of the fluid in the foam metal. The larger the permeability, the smaller the flow resistance. The structural parameters of the stainless steel foam materials selected in this study are shown in Table 2.

The pore density PPI (the average number of pores per inch length) is one of the important structural parameters of foam metal. Therefore, the influence of the pore density PPI on the heat transfer and flow performance of the new type heat transfer unit is an important research direction of this paper.

In order to study the influence of PPI changes, six numerical examples of the porosity of 0.9 and PPI of 10, 20, 30, 40, 50 and 60 are chosen. Under the condition of constant porosity, with the increase of PPI, that is, the increase in the number of pores per inch, the fiber diameter of corresponding metal foam becomes smaller, so is the pore diameter, the specific surface area increases obviously, and the permeability decreases distinctly. Therefore, as shown in Figs. 4 and 5, the pressure difference outside the tube increases sharply with the increase of PPI. At the same time, the heat transfer Rate does not increase significantly as compared with the apparent surface area, but increases slowly. This is mainly due to the fact that the thermal conductivity ratio of the nitrogen gas outside the tube to the foam metal material stainless steel is 0.00238, which is greater than 0.001, and the pore density PPI

Table 2. Structural parameters of stainless steel foam materials.

Porosity	Pore density PPI	Pore diameter d_p/m	Fiber diameter d_f/m	Specific surface area/m^{-1}	Permeability/m^2
0.95	30	0.00238	0.000287	977.713	4.296E−08
0.90	30	0.00216	0.000287	1519.952	2.740E−08
0.85	30	0.00188	0.000287	2143.183	1.615E−08
0.80	30	0.00166	0.000287	2809.302	1.020E−08
0.75	30	0.00149	0.000287	3494.713	6.965E−09
0.90	10	0.00307	0.000406	1072.533	5.504E−08
0.90	20	0.00256	0.000339	1285.173	3.833E−08
0.90	30	0.00216	0.000287	1519.952	2.740E−08
0.90	40	0.00179	0.000236	1842.434	1.865E−08
0.90	50	0.00142	0.000187	2330.671	1.165E−08
0.90	60	0.00104	0.000138	3165.209	6.319E−09

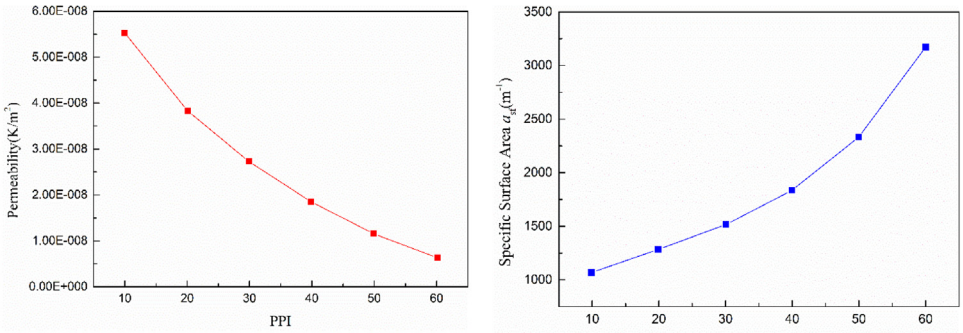

(1) Relationship between Permeability and PPI

(2) Relationship between Specific Surface Area and PPI

Fig. 5. Relationship between PPI and specific surface area and permeability.

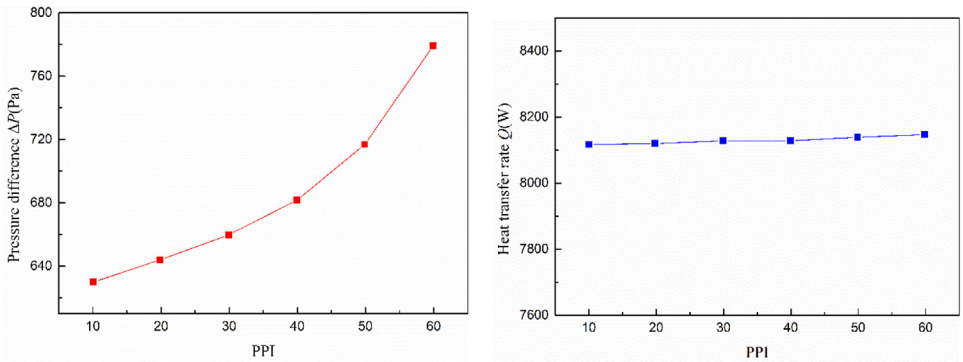

(1) Relationship between PPI and Pressure Difference in Tube Bundle

(2) Relationship between PPI and Heat Transfer Rate

Fig. 6. Relationship between PPI and pressure difference in tube bundle and heat transfer rate.

has little influence on the heat transfer coefficient within this range. This conclusion is the same as that obtained by the study of tubes filled with foam metals by W. Lu [20]. It can be seen that when k_f/k_s is 0.00238, the change of PPI has basically no effect on the change of heat transfer Rate due to the same porosity (see Fig. 6).

In order to study the influence of the change of porosity ε, the five calculation examples with PPI of 30, and the porosity of 0.75, 0.80, 0.85, 0.90 and 0.95 are selected in the numerical simulation. As shown in Figs. 7 and 8, with the increase of porosity, the specific surface area is decreased and the permeability is increased. Therefore, the heat transfer rate decreases significantly, and the pressure drop on the tube bundle side is also reduced distinctly.

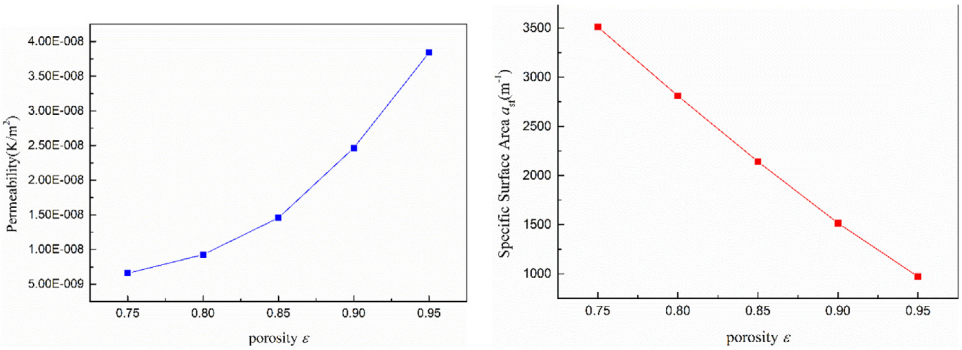

(1) Relationship between Permeability and Porosity

(2) Relationship between Porosity and Specific Surface Area

Fig. 7. Relationship between porosity and specific surface area and permeability.

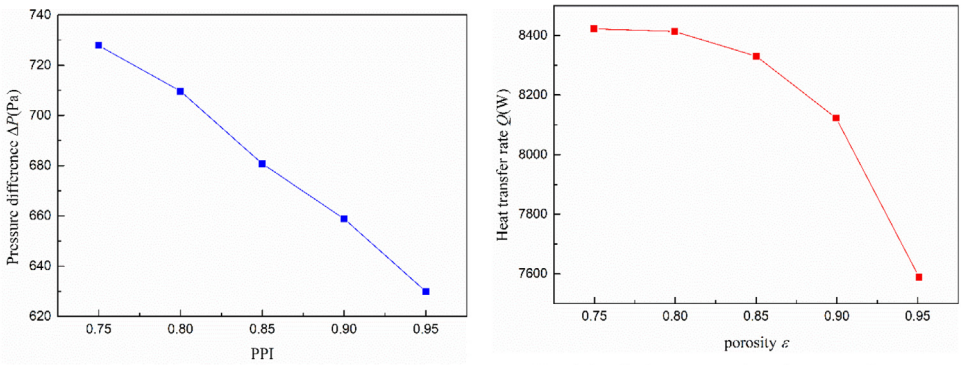

(1) Relationship between Porosity and Pressure Difference in Tube Bundle

(2) Relationship between Porosity and Heat Transfer Rate

Fig. 8. Relationship between porosity and pressure difference in tube bundle and heat transfer rate.

4. Conclusion

In this paper, the numerical simulation method is used to compare the flow field and temperature field of the smooth tube bundle and the heat transfer tube bundle of the metal foam heat absorber, and from the comparison, we are clear about the heat transfer performance and resistance performance of the two tube bundles.

The heat transfer performance of the new type heat exchange tube bundle is significantly higher than that of the smooth tube bundle. When the Reynolds number is 600, the average heat transfer coefficient of the new type heat exchange tube bundle can reach 4621 W/m^2 K. Because of the increase of the tube spacing, the pressure drop of the heat flow in the new type heat exchange tube bundle is lower than that of the smooth tube bundle. When the Reynolds number Re = 153, the pressure loss also decreases from 5.25% to 1.67%. Due to the high porosity of the metal foam, the weight of the tubes coated with metal foam inside and outside does not increase significantly, while the heat transfer Rate increases significantly, the heat transfer Rate and weight ratio of the heat exchange tube bundle rises from 1.23 to 1.59.

Declaration of competing interest

The authors declare that they have no known competing financial interests or personal relationships that could have appeared to influence the work reported in this paper.

Acknowledgments

This work was supported by Natural Science Basic Research Program of Shaanxi (Grant No. 2020JQ-1001).

References

[1] Chen K, Guo L, Xie X, et al. Experimental investigation on enhanced thermal performance of staggered tube bundles wrapped with metallic foam. Int J Heat Mass Transfer 2018;122:459–68.
[2] Chen K, Guo L, Wang H. A review on thermal application of metal foam. Sci China Technol Sci 2020;63:2469–90.
[3] Chen K, Chen P, Li W, et al. Permeation characteristics of electrodeposited metal foam. J Xi'an Jiaotong Univ 2020;54(5):87–94.
[4] Chen K, Guo L, Zhao L, et al. Experimental investigation on fluid flow and heat-transfer properties of metallic foam tube-bundle. J Eng Thermophys 2016;37(4):770–4.
[5] Calmidi VV, Mahajan RL. Forced convection in high porosity metal foams. J Heat Transfer 2000;122(3):557–65.
[6] Calmidi VV. Transport phenomena in high porosity fibrous metal foams. University of colorado; 1998.
[7] Tamayol A, Hooman K. Thermal assessment of forced convection through metal foam heat exchangers. J Heat Transfer 2011;133(11).
[8] Hooman K, Tamayol A, Malayeri M. Impact of particulate deposition on the thermohydraulic performance of metal foam heat exchangers: a simplified theoretical model. J Heat Transfer 2012;134(9).
[9] Paek J, Kang B, Kim S, et al. Effective thermal conductivity and permeability of aluminum foam materials1. Int J Thermophys 2000;21(2):453–64.
[10] Kim SY, Paek JW, Kang BH. Flow and heat transfer correlations for porous fin in a plate-fin heat exchanger. J Heat Transfer 2000;122(3):572–8.
[11] Zhao CY, Kim T, Lu TJ, et al. Thermal transport in high porosity cellular metal foams. J Thermophys Heat Transfer 2004;18(3):309–17.
[12] Zhao CY, Kim T, Lu TJ, et al. Thermal transport phenomena in porvair metal foams and sintered beds. Final Report, 2001.
[13] Mancin S, Zilio C, Cavallini A, et al. Heat transfer during air flow in aluminum foams. Int J Heat Mass Transfer 2010;53(21–22):4976–84.
[14] Mancin S, Zilio C, Rossetto L, et al. Heat transfer performance of aluminum foams. J Heat Transfer 2011;133(6):060904.
[15] Mancin S, Zilio C, Diani A, et al. Experimental air heat transfer and pressure drop through copper foams. Exp Therm Fluid Sci 2012;36:224–32.
[16] Mancin S, Zilio C, Diani A, et al. Air forced convection through metal foams: Experimental results and modeling. Int J Heat Mass Transfer 2013;62:112–23.
[17] Odabaee M, Hooman K, Gurgenci H. Metal foam heat exchangers for heat transfer augmentation from a cylinder in cross-flow. Transp Porous Media 2011;86(3):911–23.
[18] Odabaee M, Hooman K. Metal foam heat exchangers for heat transfer augmentation from a tube bank. Appl Therm Eng 2012;36:456–63.
[19] T'Joen C, De Jaeger P, Huisseune H, et al. Thermo-hydraulic study of a single row heat exchanger consisting of metal foam covered round tubes. Int J Heat Mass Transfer 2010;53(15–16):3262–74.
[20] Lu W, Zhao CY, Tassou SA. Thermal analysis on metal-foam filled heat exchangers. Part I: Metal-foam filled pipes. Int J Heat Mass Transfer 2006;49(15/16):2751–61.